Testing and characterization of an IR CBIRD FPA

Tanya Das*
*University of California, Santa Barbara
Mentor: Sir (Don) Rafol**
**Jet Propulsion Laboratory, 4800 Oak Grove Dr., Pasadena, CA 91109 USA

I. Abstract
High performance IR cameras are in great demand for a variety of applications, including defense (e.g. night vision, missile detection) and space (e.g. imaging at IR wavelengths). IR focal plane arrays (FPAs) are an essential component of IR cameras. An FPA is a collection of detectors at the focal plane of an imaging device, where each detector can be thought of a pixel in the image it is detecting. The FPA in this study is based on Complimentary Barrier Infrared Detectors (CBIRDs). The CBIRD FPA was tested by imaging flat black body targets at three different temperatures, 20ºC, 25ºC, and 30ºC, with images captured using SEIR software. The important figures of merit for an IR FPA, Noise Equivalent Difference Temperature (NEDT), Noise Equivalent Irradiance (NEI), detectivity (D*), responsivity, and quantum Efficiency (QE), were extracted from the image data for each individual detector using a MATLAB program, as was the array Modulation Transfer Function MTF. The test results show a mean NEDT of 16.98mK and an MTF of about 0.34 at the Nyquist frequency. Overall, the array performs well in the MWIR range and takes quality IR images.

Keyword: Type II Sl, CBIRD, Focal Plane Array, FPA, NEDT, NEI, D*, Responsivity, QE, MTF

II. Introduction

A. Background

Imaging in the IR occurs at three different wavelength ranges: SWIR (short-wavelength IR, 1-3μm), MWIR (mid-wave, 3-5μm), and LWIR (long-wave, 8-12μm)[1]. Currently, there are three main types of technologies which cover the MWIR and LWIR ranges: II-VI devices, III-V quantum well infrared photoconductors (QWIP), and type-II superlattice (T2SL) systems. The numbering systems (II-VI and III-V) refer to the location of elements in the periodic table. An example of an II-VI material system commonly used in IR imaging is HgCdTe, mercury-cadmium-tellurium (MCT), and an example of an III-V material system is InAs, indium arsenide. 'Type II' refers to the type of heterojunction formed between the device materials (shown in fig. 1) and 'superlattice' refers to the use of alternating layers of material during growth.

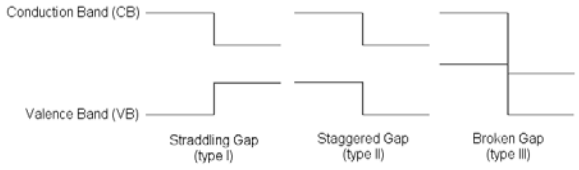

Figure 1. Types of semiconductor heterojunctions[12]

While II-VI devices perform better than QWIPs, they are also more costly to manufacture and

have issues with uniformity during fabrication. QWIPs do not perform as well as II-VI devices, but are easier to manufacture and have better uniformity[2]. Finally, the T2SL devices currently perform in a range between that of II-VI and QWIPs. Considering the availability of low cost manufacturing and uniformity in devices, the T2SL devices have great potential as IR FPAs[3].

My work this summer is to test and characterize the CBIRD array, developed at JPL. Its geometry is closest to that of a T2SL device, but has some differences (see fig. 2). CBIRD stands for Complementary Barrier Infrared Detector, and refers to the alternating quantum well structure of the device. This device geometry increases the collection efficiency of photogenerated carriers and reduces the dark current (current produced in the absence of incident light)[4].

The goals of my project are to learn how to collect relevant data on IR FPAs, write user-friendly programs to analyze the measured data to extract important figures of merit of IR FPAs, and finally to apply this knowledge to collect and analyze data on the CBIRD FPA.

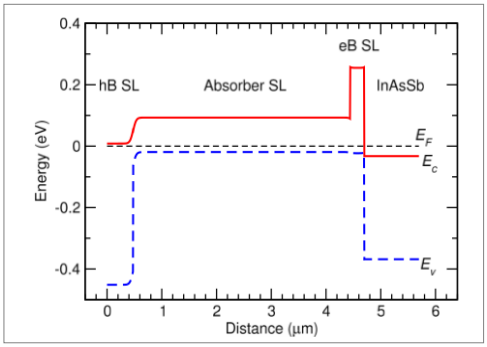

Figure 2. Band diagram of CBIRD device[4]

B. Nature of the work

There are several important figures of merit of FPAs that are extracted from the measured data, which include NEDT, NEI, QE, responsivity, D*, and modulation transfer function (MTF)[2].

A brief description of each of these parameters is as follows. The NEDT is the minimum temperature difference that is distinguishable from background noise with a signal-to-noise ratio (SNR) of one, measured in units of milli-Kelvin (mK)[3]. The NEI is the input radiant flux density required for a system that would produce an output signal equal to the noise (i.e. the input photon irradiance at which the SNR is one), measured in units of photons/second-cm^2. The quantum efficiency (QE) is the percentage of photons which impinge on the active region of the device that result in a photogenerated carrier. The responsivity is the (electrical) output/ (optical) input photon flux, measured in units of volts/photon. The detectivity is the reciprocal of the noise equivalent power (NEP). The NEP is the input optical power that will result in an SNR or one[5]. Finally, the MTF is a function which gives information about the contrast of an image relative to the contrast of the object that has been imaged. MTF can also be visualized as normalized spatial frequency response. That is, it tells how well the camera reproduces an image from the object space.

For each of the figures of merit listed above (except MTF), a MATLAB program was written to calculate the mean and standard deviation values, as well as to plot a histogram and cumulative distribution function (CDF) of the data. A bad pixel map (BPM) is also generated for each figure of merit. A bad pixel map shows the locations of pixels which lie outside a chosen tolerance range, on the order of a few standard deviations away from the mean value. For this report, bad pixels are those which lie three standard deviations or more away from the mean value. However, this can be adjusted to other requirements. All of these results are presented in section IV. Results. For details on the exact method of calculating each of these figures of merit, please see section V. Methodology: A. Calculations. All data processing was done by in MATLAB.

C. Main conclusions

This array performs well in LWIR. The main figures of merit are summarized in table 1 below.

Figure of Merit	***Mean***	***Standard deviation***
NEDT (mK)	16.98	86.12
NEI (photons/sec-cm^2)	9.84×10^{11}	4.9×10^{12}
QE (%)	26.9	2.25
Responsivity (volts/photon)	2.02×10^{-8}	1.94×10^{-9}
Detectivity (cm-Hz$^{1/2}$/W)	1.0×10^{11}	2.56×10^{10}

Table 1. Summary of figures of merit of CBIRD array

These results indicate a good quality FPA which takes clean IR images in the LWIR spectral range. The MTF shows that although there is some high-frequency noise, the FPA still takes better contrast images at higher frequencies, as can be seen in the image below[3].

Image 1. Outdoor picture taken by CBIRD array

III. Measurement setup

There are several steps necessary to prepare the FPA for data collection. First, the FPA is connected to the camera head (which interfaces between it and the computer) and is tested at room temperature for functionality. If an output is visible, the FPA is then sealed in a vacuum and tested again for functionality. If the FPA is still functioning properly, it is cooled to 80K with liquid nitrogen and then data collection can ensue. The camera detects lower temperatures targets better as it cools. The various figures of merit described in the section II. B. is all extracted from black body image data[6]. For the purposes of this experiment, a black body can be described as an emitter which emits a constant temperature across its entire surface. Using the CR-80 black body source, we are able to precisely control the temperature of a black body emitter, and image the black body with our FPA. We collect data by imaging a flat black body at three different temperatures. The images that are taken record the brightness (or 'count') at each pixel in the array. A higher brightness means a higher temperature at that pixel. Typically, several frames of images are taken at each black body temperature, and then averaged at each pixel during processing to extract the relevant figures of merit (again, details are in section V. A.). Using a CR-80 black body source and SEIR software, one hundred frames of images were collected at three blackbody temperatures: 20°C, 25°C, and 30°C. The data from the first 32 frames were averages and used during processing. The temporal noise is estimated at the 25C.

The MTF is extracted by collecting data from the image of a 'knife-edge target' illuminated by a blackbody. A knife-edge target is a target which has a very sharp edge, so half of the image is brightly lit and half is completely dark. Analyzing the sharpness of the transition between the bright and dark regions gives the MTF. The knife-edge image was produced using a four-bar target in front in a black body source.

IV. Results

A. Images and histograms

The images collected at the various black body temperatures are shown in fig. 3, along

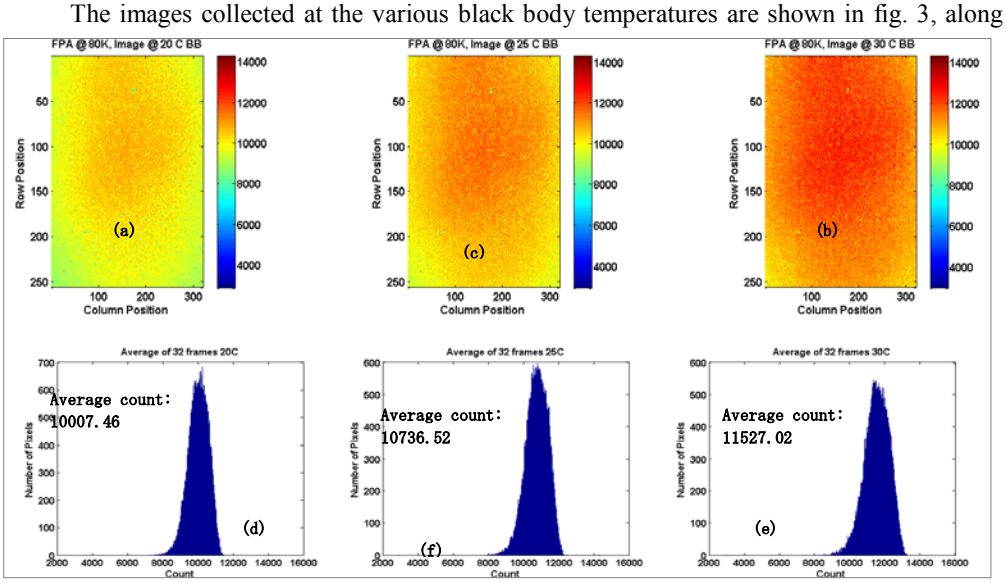

with histograms of the count data.

Figure 3. Black body images and histograms at 20°C, 25°C, and 30°C (left to right)

As can be seen from fig. 3a, 3b, and 3c, the brightness of the images gradually increases as the temperature of the black body image increases. This result corresponds with our expectations, as a warmer object should produce a brighter image. We also notice from looking at fig. 3d, 3e, and 3f that the peak of the image histogram moves to the right as the black body temperature increases. This result also corresponds with our expectations, since a brighter image should have more pixels with higher counts.

B. NEDT

The NEDT histogram, CDF and BPM (with bad pixels highlighted in white, and circled in red for reference) are shown in fig. 4. As can be seen from fig. 4, the mean NEDT value is quite low, at 16.98mK. The value calculated from the data is in good agreement with the NEDT value calculated by the SEIR software, which is 19mK (10.6% error). The NEDT distribution is tight, although there is a somewhat significant tail at higher NEDT values. However, generally these are good NEDT results, and there are only three bad pixels, all of which lie above 3σ.

Formatted: Font: (Default) Times New Roman

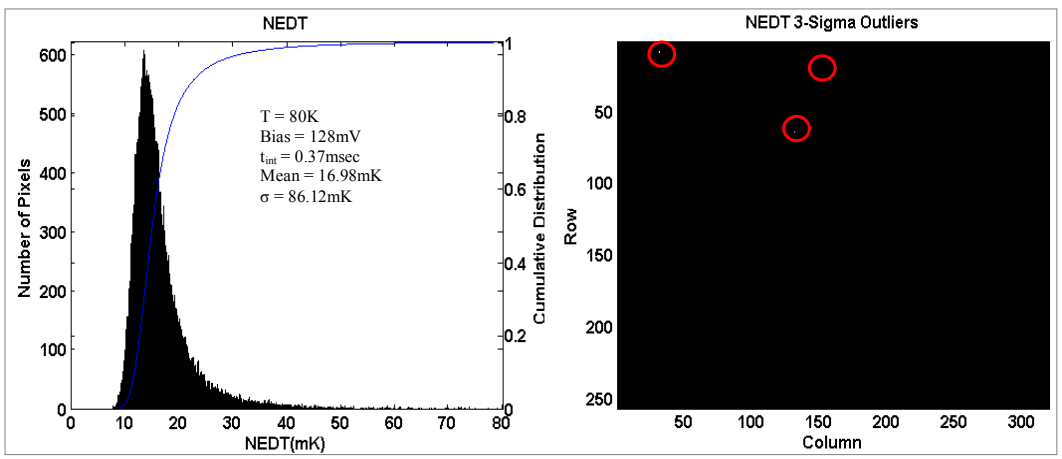

Figure 4. NEDT histogram, CDF, and BPM

C. NEI

The NEI histogram, CDF and BPM are shown in fig. 5. As can be seen from fig. 5, the mean NEI value is quite high, at 9.84×10^{11} photons/sec-cm^2. The NEI distribution is somewhat tight, though again there is a somewhat significant tail at higher NEI values. However, generally these are good NEI results. The NEI and NEDT bad pixel maps should match, and as shown here, indeed they do. There are again only three bad pixels.

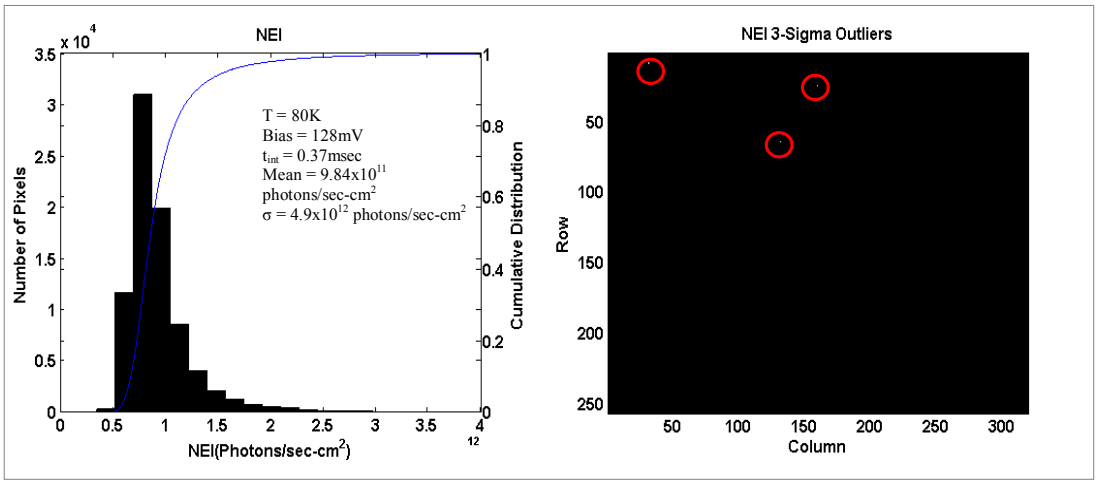

Figure 5. NEI histogram, CDF, and BPM

D. QE

The QE histogram, CDF and BPM (with bad pixels highlighted in white) are shown in fig. 6. As can be seen from fig. 6, the mean QE is about 27%, which is a reasonable value. The QE distribution is rather tight, as is evident from the small standard deviation value. However, there are many more bad pixels in the QE map than in the NEDT and NEI maps. There are 1384 bad

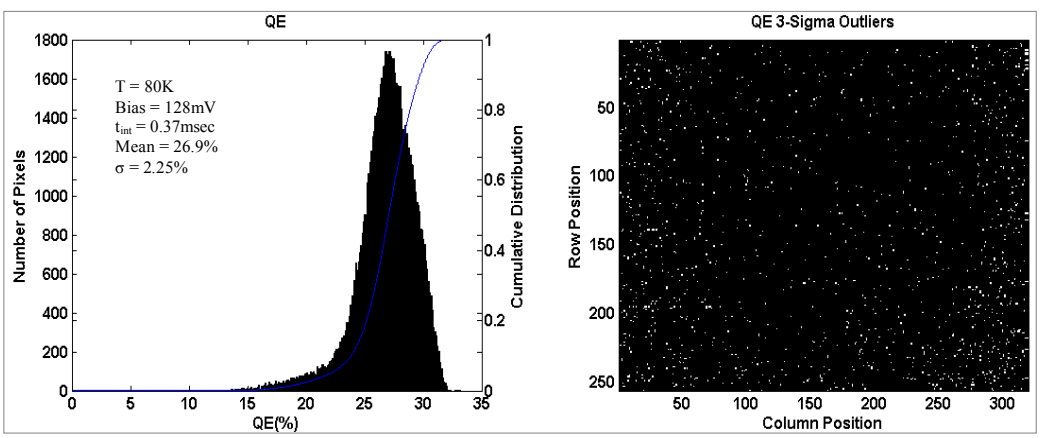

pixels, all of which lie below 3σ.

Figure 6. QE histogram, CDF, and BPM

E. Responsivity

The responsivity histogram, CDF and BPM are shown in fig. 7. As can be seen from fig. 7, the mean responsivity is 2.02×10^{-8} volts/photon, which is a reasonable value, and the distribution is rather tight. As the responsivity BPM should match the QE BPM, there are again a large number of bad pixels.

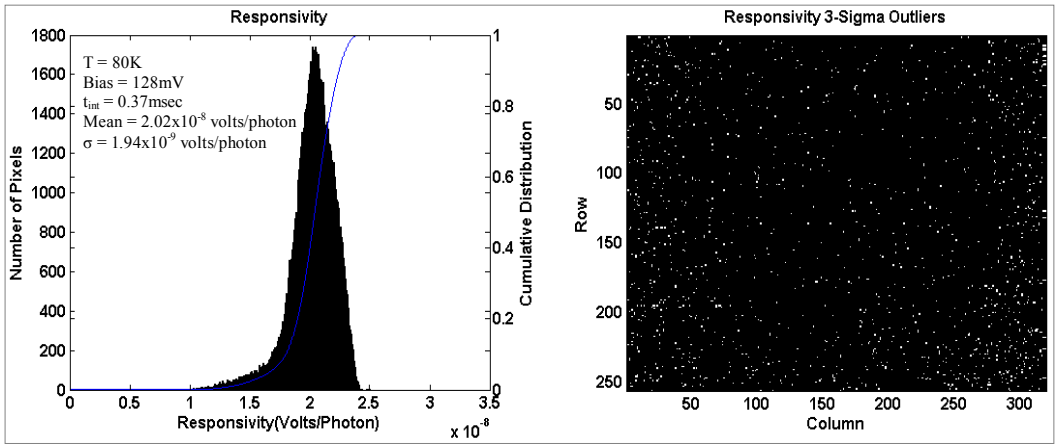

Figure 7. Responsivity histogram, CDF, and BPM

F. D*

The detectivity histogram, CDF and BPM are shown in fig. 8. As can be seen from fig. 8, the mean detectivity is 1.0x10^{11} cm-Hz$^{1/2}$/W, which is a reasonable value. There are 10 bad pixels, all of which lie below 3σ.

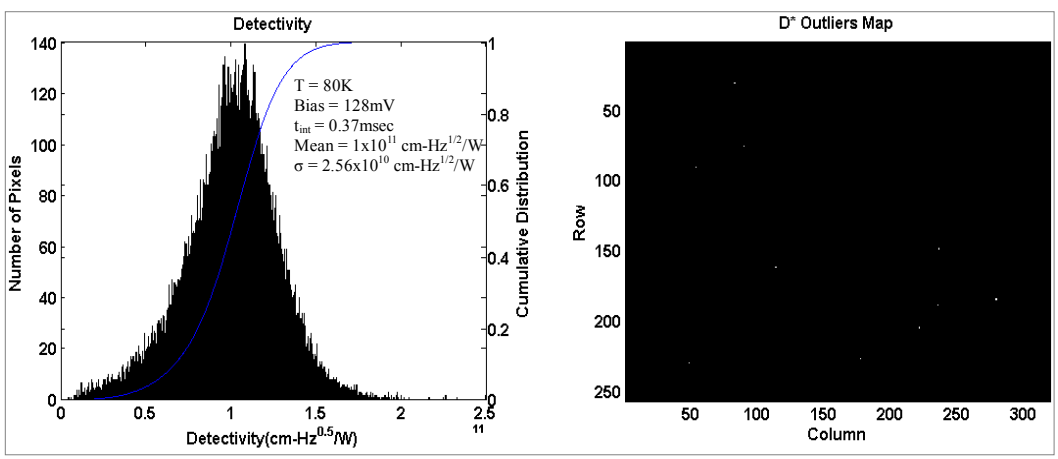

Figure 8. Figure 7. D* histogram, CDF, and BPM

G. MTF

As mentioned previously, the MTF is extracted from the image of a knife-edge target. In this study, a four-bar target was used in front of a black body source. However, the blackbody background was nonuniform, as is seen in fig. 9.

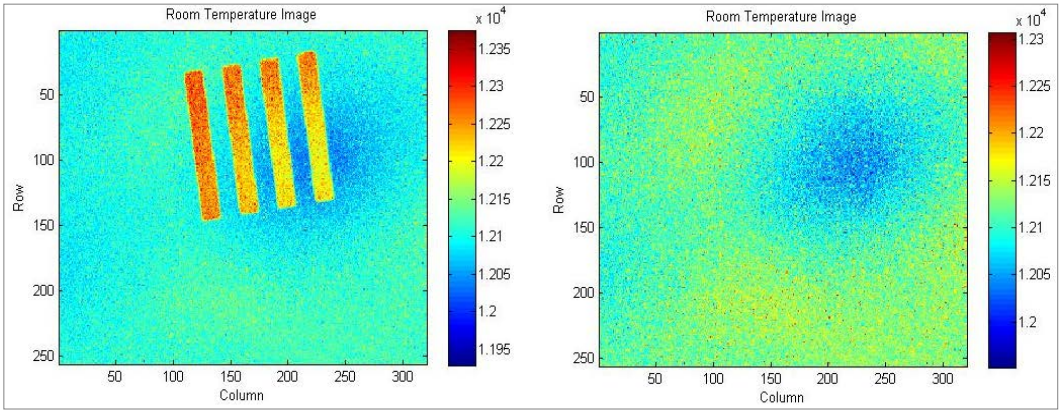

Figure 9. Knife-edge image (left) and background image (right)

Thus a blank image of the background had to be taken (see fig. 9) and then subtracted from the original image to produce a final image, from which the MTF was extracted. The final image, along with its histogram, is shown in fig. 10.

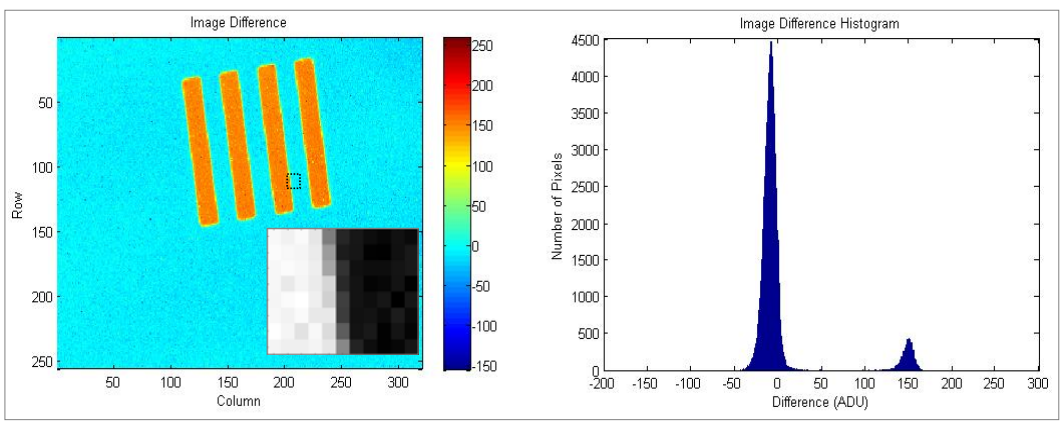

Figure 10. Knife-edge with background subtracted with boxed ROI in inset (left) and image histogram (right)

There are two methods for extracting the MTF investigated in this study: the periodic method and Quick MTF method. For both of these methods, the same region of interest (ROI) was used to extract the MTF, which is the boxed region shown in fig. 10. A slightly smaller region within this ROI was selected for the periodic method (shown in the gray scale inset), as this method relies on the periodicity in the knife-edge image. For a description of the two MTF methods, as

well as an explanation of the methods for calculating the edge spread function (ESF), line spread function (LSF), and MTF, please see section V. Methodology: C. MTF.

The ESF and LSF are also shown in fig. 11, where the original data is in blue, the Fermi function fitted data is shown in red, and the Quick MTF (commercial analysis software) data is shown in green. Evidently, the Fermi function provides a good fit to the edge spread function data.

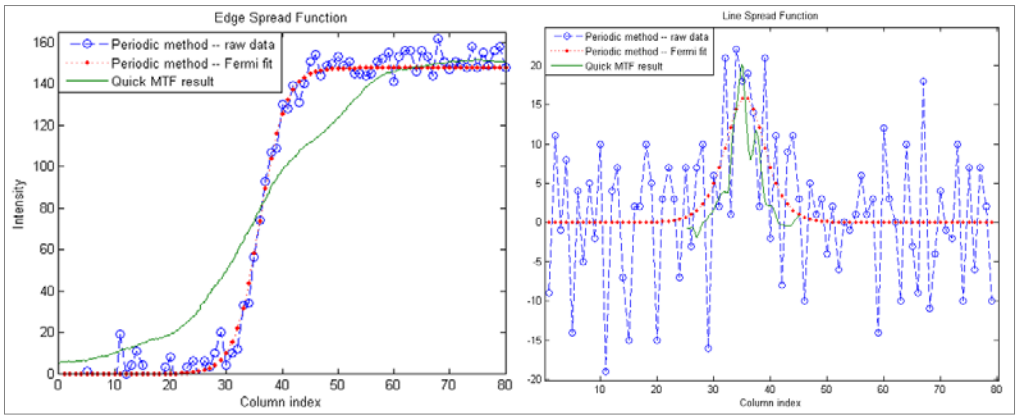

Figure 11. ESF (left) and LSF (right): raw data in red, Fermi fit in blue, and Quick MTF in green

The Fermi fit for the ESF results in a very clean MTF at low frequencies, as shown in fig. 12. Clearly, the Fermi function model fits the data quite well at low frequencies. At the Nyquist frequency (16.67 cyc/mm), the MTF is still nonzero (~0.34), which indicates that he FPA should still respond well to high-frequency image variations[6]. Dividing by 0.59 for the lens MTF at Nyquist , result to about 57 % MTF for the detector.

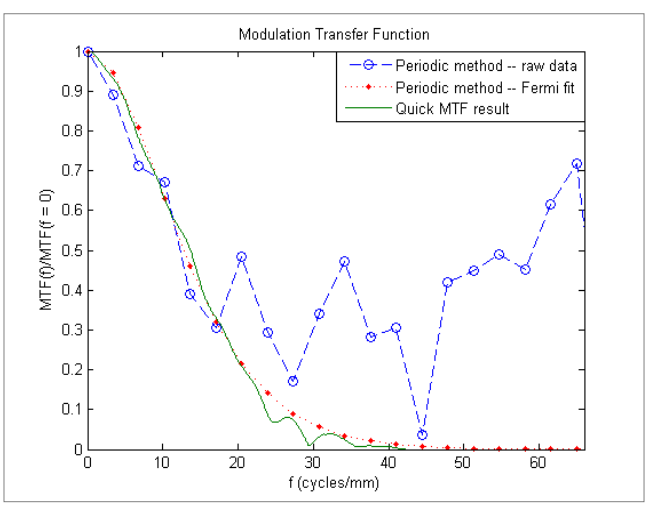

Figure 12. MTF: raw data in red, Fermi fit in blue, and Quick MTF in green

V. Methodology

A. Calculations

i. NEDT

The NEDT is a figure of merit that describes the performance of a thermal imaging system. Basically, it is the minimum temperature difference that is distinguishable from background noise with a signal-to-noise ratio of one[3]. The (spatial and temporal) NEDT can be derived from the spatial and temporal noise and the responsivity of the FPA[6].

Spatial noise is a nonuniformity in an image due to pixel-to-pixel variations in the array. When looking at an FPA image, it will appear as a constant pattern on the image, regardless of what the FPA is imaging. We can use data processing techniques (see the section on NUC) to remove these unwanted variations. Temporal noise is random in nature and changes with each new frame taken by the FPA[7]. The temporal NEDT is the more relevant parameter. The temporal NEDT is calculated as follows,

$$NEDT = \frac{\sigma_{temporal} * \Delta T}{Mean(T_H) - Mean(T_L)}$$

where $\sigma_{temporal}$ is the temporal noise, ΔT is the temperature difference between the high and low black body images, and Mean(T_H) Mean(T_L) are the averages at the high and low black body temperatures (T_H and T_L respectively) over a user-specified number of frames *N,* and give the average value at each data point. The 'count' refers to the brightness of the signal detected by each pixel in the array. The temporal noise is calculated as follows,

$$\sigma_{temporal} = \sum_{n=1}^{n=N} \sqrt{\frac{(average_{ij} - data_{ij})^2}{N}}$$

where $average_{ij}$ is the average count value at the point i,j, taken over a user-specified number of frames *N*, and $data_{ij}$ is the data count value at the point i,j in frame *n*. In this study, the average data was always calculated from the middle black body -temperature data (25ºC), but can be calculated from any of the black body temperature data.

ii. NEI

The NEI is the radiant flux density required for a system to produce an output signal equal to the noise (i.e. the input photon irradiance at which the SNR is one), measured in units of photons/second-cm^2. The NEI is calculated in the following way:

$$NEI = \frac{T * \Delta\Phi_{photon} * NF * \sigma_{temporal}}{Mean(T_H) - Mean(T_L)}$$

where T is the transmission, $\Delta\Phi$ is the photon flux between T_H and T_L, and NF is the noise factor. Φ is calculated by the program and NF is user-defined.

iii. QE

The QE is the percentage of photon carriers which impinge on the active region of the device that result in a photogenerated carrier. The QE is calculated in the following way:

$$QE = \frac{V_{ADC} * (Mean(T_H) - Mean(T_L))}{Gain_{ROIC} * t_{int.} * \Delta\Phi_{photon} * A * NF}$$

where V_{ADC} is the ADC voltage, $Gain_{ROIC}$ is the gain of the ROIC (read-out-integrated circuit), $t_{int.}$ is the integration time, and A is the area of the array in cm^2. Integration time is the amount of time that the FPA is exposed to the image, and is defined by the user in the SEIR measurement program when the image data is collected. The ROIC gain is given in the ROIC specifications.

iv. Responsivity

The responsivity is the (electrical) output/ (optical) input gain, measured in units of volts/photon. The responsivity is calculated as follows,

$$Responsivity = \frac{V_{ADC} * (Mean(T_H) - Mean(T_L))}{T * t_{int.} * \Delta\Phi_{photon} * A}$$

v. Detectivity

The detectivity is the reciprocal of the noise equivalent power (NEP). The NEP is the input optical power that will result in an SNR or one[5]. The units of detectivity are cm-$Hz^{1/2}$/W, and it is detectivity is calculated in the following way:

$$D = \left(\sqrt{\frac{A}{2 * t_{int.}}} * \frac{Responsivity}{Noise} \right)$$

B. Non-uniformity correction (NUC)

As was mentioned previously, the spatial noise in a FPA image can be corrected so the nonuniformities no longer appear in the final processed image, and we use a non-uniformity correction (NUC) algorithm to correct the image. We assumed that the spatial noise is independent of time.

The NUC algorithm assumes the responsivity of each pixel to be linear, so the goal when applying correction is to find the y = mx+b line that describes the behavior of each pixel. Therefore, the gain ('m', slope) and offset ('b', y-intercept) need to be calculated for every pixel in the array in order to apply the correction. We require only two points in order to define the equation for a line, so we take two images of constant temperature with the array and calculate the gain and offset from this data in the following way:

$$Gain = \frac{Mean(T_H) - Mean(T_{Low})}{High_{ij} - Low_{ij}}$$

$$Offset = \frac{Mean(T_H) + Mean(T_L)}{2} - \frac{gain * (High_{ij} + Low_{ij})}{2}$$

The method above is called the two-point NUC. Over time, the array may heat up or cool down, or various environment changes may cause drifting of the pixel offset values. A one-point correction is then periodically required to reestablish a good quality image. To perform a one-point correction, we take one image of constant temperature with the array and calculate only the offset, in the following way (where the gain was previously specified from the two-point NUC):

$$Offset = Mean(T) - \frac{gain * T_{ij}}{2}$$

Here you can see the difference between an uncorrected and a corrected image. The corrected image on the right appears very clean, even though the uncorrected image on the left appears to have some irregularities.

Image 2. Uncorrected FPA image (left) and corrected image with NUC applied (right)

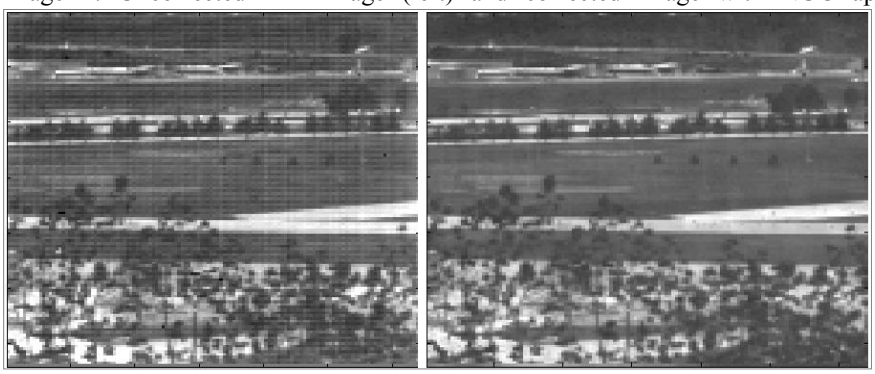

C. MTF

There are two different methods of MTF calculation examined in this paper: periodicity and Quick MTF. The periodic method is explained in detail in reference [9], but essentially involves oversampling the edge spread function by taking the edge data over one period of the knife edge image. This periodicity is evident in the inset of figure 10.

The Quick MTF method for calculating the MTF is the traditional method, which involves sampling edge data directly across the image edge over the entire ROI, and then rearranging the

data points to determine the ESF. Details are given in reference [10].

For both methods, the LSF is extracted by taking the point-by-point derivative of the ESF. The MTF is simply the Fourier Transform of the LSF.

VII. Acknowledgements

This research was carried out at the Jet Propulsion Laboratory, California Institute of Technology, and was sponsored by California Space Grant and the National Aeronautics and Space Administration Special thanks to Don Rafol for being a very patient and helpful mentor, and to California Space Grant for funding my work this summer.

VIII. References

[1] J. Byrnes, *Unexploded Ordnance Detection and Mitigation,* Springer (2009) 21–22.

[2] A. Rogalski, "Recent progress in infrared detector technologies", Proceedings of the International Conference on Quantum Structure Photodetectors (QSIP) 2010, Infrared Physics & Technology 54 (2011) 136-154.

[3] S.B., Rafol, A. Soibel, A. Khoshakhlagh, J. Nguyen, J.K. Liu, J.M. Mumolo, S.A. Keo, L. Hoglund, D. Z. Ting, S.D. Gunapala, "Performance of a 1/4 VGA Format Long-Wavelength Infrared Antimonides-Based Superlattice Focal Plane Array," IEEE Journal of Quantum Electronics, 48 (2012) 878-884.

[4] D.Z.. Ting, C. Hill, A. Soibel, S.A. Keo, J.M. Mumolo, et. al., "A high-performance long wavelength superlattice complementary barrier infrared detector," Appl. Phys. Lett. 95, 023508 (2009).

[5] P.L. Richards, "Bolometers for infrared and millimeter waves", Journal of Applied Physics, 76, 1 (1994).

[6] M. J. Burke and W. Wan, "IR FPA sensor characterization and analysis using MATLAB," Proc. SPIE, 3377 (1998) 1–71.

[7] J. Mooney, "Effect of spatial noise on the minimum resolvable temperature of a staring sensor," Appl. Opt. 30 (1991) 3324-3332.

[8] P. Delaunay and M. Razeghi, "Spatial Noise and Correctability of Type-II InAs/GaSb Focal Plane Arrays", IEEE Journal of Quantum Electronics, 46 (2010) 584-588.

[9] S. B. Rafol and E. Cho, "Modulation transfer function measurement on QWIP focal plane array", Proc. SPIE 6941, 69410X (2008).

[10] Quick MTF, Basic steps in calculating the MTF (SFR),

http://www.quickmtf.com/slantededge.html (accessed 13 August 2012).

[11] NUC group at Universidad de Conception, Chile. http://nuc.die.udec.cl/?page_id=18 (accessed 13 August 2012).

[12]HeterojunctionTypes,Wikipedia.
http://upload.wikimedia.org/wikipedia/en/1/1d/Heterojunction_types.png (accessed 13 August 2012).